High Resolution Observations of the Elliptical Galaxy NGC 4636 with the Reflection Grating Spectrometer On-Board XMM-Newton

H. Xu[1,2], S. M. Kahn[1], J. R. Peterson[1], E. Behar[1],

F. B. S. Paerels[1], R. F. Mushotzky[3], J. G. Jernigan[4],

and K. Makishima[5]

[1] *Columbia Astrophysics Laboratory, 550 W 120th Street, New York, NY 10027, USA*

[2] *Department of Applied Physics, Shanghai Jiao Tong University,*

1954 Huashan Road, Shanghai 200030, PRC

[3] *NASA/GSFC, Code 662, Greenbelt, MD 20771, USA*

[4] *Space Sciences Laboratory, University of California, Berkeley, CA 94720, USA*

[5] *Department of Physics, University of Tokyo, 7-3-1 Hongo, Bunkyo-ku, Tokyo 113-0033, Japan*

Received ______________________; accepted ______________________

ABSTRACT

We present the first high spectral resolution X-ray observation of the giant elliptical galaxy NGC 4636, obtained with the Reflection Grating Spectrometer on-board the XMM-Newton Observatory. The resulting spectrum contains a wealth of emission lines from various charge states of oxygen, neon, magnesium, and iron. Examination of the cross-dispersion profiles of several of these lines provides clear, unambiguous evidence of resonance scattering by the highest oscillator strength lines, as well as a weak temperature gradient in the inner regions of the interstellar medium. We invoke a sophisticated new Monte Carlo technique which allows us to properly account for these effects in performing quantitative fits to the spectrum. Our spectral fits are not subject to many of the systematics that have plagued earlier investigations. The derived metal abundances are higher than have been inferred from prior, lower spectral resolution observations of this source (Awaki et al. 1994), but are still incompatible with conventional chemical enrichment models of elliptical galaxies. In addition, our data are incompatible with standard cooling flow models for this system - our derived upper limit to the mass deposition rate is below the predicted value by a factor of 3–5.

Subject headings: galaxies: individual (NGC 4636)–galaxies: ISM–X-rays: galaxies

1. Introduction

Most elliptical and other early-type galaxies possess a hot and diffuse interstellar medium (ISM) that extends out to several tens of kpc. The ISM temperature ranges from 0.5 keV to 1 keV (e.g., Matsumoto et al. 1997) so that most of its emission is radiated in

the soft X-ray band. Detailed analysis of the X-ray spectra of these systems, which are dominated by a wealth of characteristic emission lines, provides a robust tool to understand the metal enrichment processes in stars and interstellar gas, and possibly to constrain the supernova history of the parent galaxies.

However, in all previous investigations, the spectral resolution and/or sensitivity of the instruments used were insufficient to cleanly address these issues. Hundreds of emission lines, particularly a forest of iron-L lines, were completely blended in the observed spectra. Therefore, simple model fits to the X-ray data do not yield unambiguous determinations of the gas density and temperature, the metal abundances, or their spatial distributions.

In this paper, we report the first high spectral resolution X-ray observation of the giant elliptical galaxy NGC 4636, performed with the Reflection Grating Spectrometer (RGS) (den Herder et al. 2001) on board the XMM-Newton Observatory. At $z = 0.003129$ (Smith et al. 2000), NGC 4636 is located in the skirt region of the Virgo cluster. Global fitting of ASCA SIS spectra (Matsumoto et al. 1997) yielded a mean temperature for the interstellar gas in this galaxy of 0.76 ± 0.01 keV and an average metal abundance of $0.31^{+0.04}_{-0.03}$ solar. The $0.5 - 4.5$ keV luminosity was found to be 5.7×10^{41} erg s^{-1} which makes it one of the brightest elliptical galaxies in the X-ray band.

In §2, we describe our observations and basic data reduction procedures. The detailed analysis of the RGS spectrum is presented in §3. We demonstrate that the observed spectral and spatial distributions mandate the presence of a weak temperature gradient in the ISM of NGC 4636, as well as careful consideration of the importance of resonance line scattering in interpreting the measured line intensities. We invoke a novel modeling and fitting procedure that allows us to constrain the relevant plasma parameters with these effects included. Our spectral fits indicate higher metal abundances than have been inferred from prior, lower spectral resolution observations of this source, but are still discrepant

with expectations from conventional chemical enrichment models. In addition, we place tight upper limits on the contribution of low temperature gas, in contradiction with the predictions of standard cooling-flow models for the ISM of this galaxy. In §4, we summarize and discuss the implications of these results. Throughout the paper, we assume a distance to NGC 4636 of 15.0 Mpc (Ferrarese et al. 2000). Unless stated otherwise, the wavelengths of the emission lines are expressed in a reference frame at rest in the source. The solar abundance ratios are taken from Anders and Grevesse (1988).

2. Observations and Data Reduction

NGC 4636 was observed with XMM-Newton in revolutions 0109 (July 13–14, 2000) and 0197 (January 5, 2001). During revolution 0109, a historically strong solar flare event occurred so that the European Photon Imaging Camera (EPIC) detectors were all switched off, and the RGS spectra were heavily contaminated with particle-induced background. In this initial report, we therefore concentrate on the RGS data obtained during the second observation. The total exposure is approximately 64 ks. We processed the data with the Science Analysis System (SAS) for event reconstruction, CCD energy correction, and angular coordinate mapping. Approximately 3.5×10^4 photons are contained in the spectrum after rejecting bad events. Given the spatial extent of the source, the effective spectral resolution of the RGS is $\Delta\lambda \sim 0.2$ Å over most of the band.

3. Spectral Analysis

3.1. Line Identification

The raw RGS spectra, which are uncorrected for the response of the instrument and the redshift of the source, are plotted as a function of wavelength in Figure 1. The first-

and second-order spectra obtained by both RGS1 and RGS2 have been added together in constructing this figure. We have not removed particle or detector background. The spectra are dominated by the $2p - 3d$ lines of Fe XVII-XXI ($12 - 15$ Å), the $2p - 3s$ lines of Fe XVII-XVIII ($16 - 17.1$ Å), and the Lyα lines of O VIII (19.0 Å) and Ne X (12.1 Å). The blended Helium-like Mg XI triplet (~ 9.2 Å) can also be clearly identified. In addition, there are weak Lyα lines of N VII (24.8 Å) and Mg XII (8.4 Å), and the O VII triplet at $21.6 - 22.1$ Å. Because the O VIII lines are much stronger than the O VII lines, and the Fe XVIII-XIX $2p - 3d$ lines are weaker than the Fe XVII $2p - 3d$ lines, there must be very little contribution from gas with $kT < 500$ eV or $kT > 700$ eV. The ratios of Mg XII line intensities to those of Mg XI are consistent with this range, and in fact indicate a temperature of approximately 600 eV.

Measured incident fluxes of those lines which can be well isolated are given in Table 1. These have been obtained by integrating over the cross-dispersion direction on the RGS detectors, subtracting the relevant background, and dividing by both the RGS effective area specific to these extractions and by the effective exposure times. Of particular interest are the relative intensities of the brightest Fe XVII lines at 15.01 Å, 15.26 Å, 16.78 Å, and those at 17.05 and 17.10 Å, which are blended. Ratios of these lines are listed in Table 2, along with the analogous quantities deduced from Chandra HETG observations of Capella (which has a very similar temperature to what we infer for NGC 4636; Behar et al. 2001), and the predicted line ratios at this temperature given by the APEC model for a plasma in collisional equilibrium (Smith et al. 2001). As can be seen, the NGC 4636 Fe XVII line ratios are in reasonable agreement with those measured for Capella, but disagree more significantly with the APEC predictions. We find similar effects for Fe XVIII. In both cases, the $2p - 3d$ lines are too weak relative to the $2p - 3s$ lines. The origin of this discrepancy is still unclear, but, since it is also observed in the Capella spectrum, it appears to possibly be an artifact of uncertainties in the atomic excitation rates for these lines (Brown et al. 1998;

Laming et al. 2000; but see also Brown et al. 2001), and not of the astrophysical conditions in the NGC 4636 ISM. We therefore empirically correct the intraseries Fe L-shell line ratios in our subsequent modeling, using Capella as the calibrator. Following Behar et al. (2001), we choose to normalize the relative line intensities to the intensity of the 15.26 Å line for Fe XVII and its spectroscopic equivalent for Fe XVIII. This choice gives the best agreement with the remainder of the L-shell complex for each ion, particularly the higher series lines.

3.2. Cross-Dispersion Profiles

The RGS is a slitless, nearly stigmatic spectrometer, which means we can place some constraints on the spatial dependence of the various emission lines, by examining the profile of the emission line fluxes and their ratios in the cross-dispersion direction. We first look at the ratio of the two $2p-3s$ lines of Fe XVII at 17.1 Å to that of the $2p-3d$ line of Fe XVII at 15.0 Å, which is plotted in Figure 2a. As can be seen, this ratio is significantly peaked toward the center of the gaseous halo of the galaxy. Since these lines originate from the same charge state of a single element, the observed spatial dependence cannot be due to gradients in either the temperature or elemental abundances within the ISM. Instead, it is most likely produced by resonance line scattering of the 15.0 Å photons. The oscillator strength for the $2p-3d$ transition is substantially higher than that of the $2p-3s$ lines. For the inferred densities and temperatures in the core of the NGC 4636 ISM, the 15.0 Å line optical depth is greater than unity, while the 17.1 Å blend optical depth is negligible. The 15.0 Å photons typically scatter one or more times before exiting the medium, flattening the intensity profile of that line in comparison to the others. Hence, accurate treatment of resonance line scattering is essential to correctly modeling the extracted spectrum. [1]

[1] In deriving the line intensities given in Tables 1 and 2, we used an extraction region of $2'$ in the cross-direction. Since this is much larger than the angular scale of the observed

In Figure 2b, we plot the ratio of the 17.1 Å line of Fe XVII to the 16.0 Å line of Fe XVIII. Here again, it is centrally peaked. However, these are both $2p - 3s$ transitions, and neither has sufficient optical depth for the profile to be affected by resonance scattering. In this case, the variation in the ratio must be associated with a temperature gradient, which makes the Fe XVII and Fe XVIII ion fractions a function of radius. The temperature must drop by $\sim 20 - 30$ percent from the outer regions of the halo toward the core.

Finally, in Figure 2c, we plot the ratio of the Fe XVII 17.1 Å blend to the Lyα line of O VIII at 19.0 Å. These lines have similar, but not exactly identical emissivity dependences on temperature. As can be seen, there is only a mild spatial dependence, of the same order as expected for the inferred temperature gradient. The implication is that there is not a severe relative abundance gradient in the halo. We also find no strong evidence of abundance gradients by looking at the profiles of line ratios involving the other elements.

3.3. Quantitative Spectral Fitting

As we have shown, proper modeling of the gas distribution in the ISM of NGC 4636 requires careful treatment of both temperature gradients and resonance line transfer. In addition, since this is an extended source, the line spread function of the RGS instrument is dependent on the spatial distribution of the emission. All of these factors require that the spatial and spectral distributions be modeled jointly. Standard spectral fitting procedures cannot be used for this purpose.

We have developed a new approach to spectral fitting of extended sources which relies on Monte Carlo methods (Peterson, Jernigan, & Kahn 2001). Assuming given 3-dimensional spatial distributions for the relevant plasma parameters, Monte Carlo

---

variations, resonance scattering does not affect these integrated line intensities.

photons are generated within the medium at positions and wavelengths weighted by the emissivity model. These photons are then scattered in both frequency and space based on line scattering probabilities, evaluated assuming velocity widths appropriate to maxwellian doppler broadening at the local gas temperature. At each scatter, the photon is given a new trajectory and frequency until it escapes from the model medium. After projection onto the sky, the photons are propagated through an instrument Monte Carlo simulator to predict the eventual detected position in both the dispersion and cross-dispersion coordinates, and the CCD charge content of the event. A separate Monte Carlo algorithm, calibrated on deep observations of the Lockman Hole, is used to generate an appropriate sample of background events. The final simulated data set is subjected to the identical set of extractions as are applied to the measured data. The observed and simulated data are compared by means of a χ^2 statistic in each of the various dimensions. This process is repeated by iterating on the parameters characterizing the spatial and spectral distributions until an acceptable fit is obtained. In order to maintain high accuracy in the simulation, the number of simulated photons is chosen to be ten times higher than that of the observed data set.

We assume a β profile (Cavaliere & Fusco-Femiano 1976) to approximate the spatial distribution of the electron density within the central 2':

$$n(R) = n_0 \left[1 + (R/R_c)^2\right]^{-3\beta/2} . \tag{1}$$

The core radius, R_c, and the β parameter were determined from fits derived from an available Chandra ACIS observation (Mushotzky et al. 2001), and were found to be 9" and 0.45 respectively. The central density, n_0, is left as a free parameter. To accommodate the observed temperature gradient, we assume a temperature distribution of the form:

$$T(R) \;=\; \begin{cases} T_{\rm min} + (T_{\rm max} - T_{\rm min})(\frac{R}{R_c})^\alpha & \text{if } R \le R_c \\ T_{\rm max} & \text{if } R > R_c \end{cases} \tag{2}$$

with α, $T_{\rm min}$, and $T_{\rm max}$ left as free parameters.

To model the gas emissivity, we use the APEC model, with the Fe L-shell $2p - 3s$ to $2p - 3d$ ratios adjusted to match the Capella values, as discussed in §3.1. The abundances of N, O, Ne, Mg, and Fe (which account for all of the observed features in the spectrum) are left as free parameters. The best fit values of all of these parameters are listed in Table 3. Here, the value of χ^2 quoted is for the comparison to the spectrum displayed in Figure 1, where the model has been overlayed. As can be seen, the fit is quite good. There are only small residuals in the vicinities of the brightest lines, possibly indicating that the assumed β-profile may still be too much of an over-simplication. The predicted cross-dispersion profiles for this same model are also plotted in the various panels of Figure 2. In general, there is excellent agreement with the data. We have not allowed for any abundance gradients in the model, and none appear to be required. The best-fit temperature distribution increases gradually from $kT = 0.55$ keV at $R = 0$ to $kT = 0.70$ keV at $R = 42$". With this temperature profile, the observed temperature-sensitive $I(17.1\text{Å})/I(16.0\text{Å})$ ratio is fitted very well (Figure 2b).

Note that the $I(17.1\text{Å})/I(15.0\text{Å})$ ratio is also well-described by the model (Figure 2a). This validates our conjecture that the observed variation in this ratio is associated with resonance scattering of the 15.0 Å photons. We emphasize that the gas density was not independently adjusted to fit this variation, i.e. the same density profile necessary to describe the observed intensity distribution (at the same assumed distance) also quantitatively accounts for the observed resonance scattering effects. In addition, our derived value for the central gas density is in good agreement with that found by Loewenstein et al. (2001) for the bremsstrahlung continuum in the Chandra ACIS spectrum.

In these spectral fits, no extra absorption beyond that associated with the Galactic column, $N_{\rm H} = 1.87 \times 10^{20}$ cm^{-2} (Murphy et al. 1996), is required. With our best-fit parameters, we find that the total X-ray luminosity within 1' is $1.87 \pm 0.19 \times 10^{41}$ erg s^{-1}.

This agrees well with the ROSAT (Matsushita 2001) and the recent Chandra (Loewenstein et al. 2001) measured values.

We have not attempted to develop and fit a full spatial-spectral cooling flow model for NGC 4636. However, important constraints on cooling flow models can be derived from the observed luminosities in the Fe XVII and O VII emission lines. The multiphase, isobaric cooling flow model of Johnstone et al. (1992) predicts a constant luminosity per temperature interval that is proportional to the mass deposition rate of cooling gas. This radiation is in addition to that emitted by the ambient gas, which has not yet cooled. Individual spectral line fluxes can thus be used to derive upper limits to the mass deposition rate, applicable within particular temperature ranges of sensitivity.

Assuming the β-profile described above, our observed Fe XVII line intensities imply an upper limit to the mass deposition rate of 0.21 $M_{\odot}$ yr^{-1}. Assuming that iron L-shell emission dominates the cooling of the gas, which is true in this temperature range, this derived limit on the mass deposition rate is relatively insensitive to the iron abundance. That is not true for oxygen. However, we can fix the O/Fe abundance ratio using the relative intensity of the O VIII Lyα line. With that constraint, the measured O VII line intensities near 22 Å imply an upper limit on the cooling flow mass deposition rate of 0.30 $M_{\odot}$ yr^{-1}. Note that these limits are a factor 3–5 below the inferred theoretical mass deposition rates for the halo of this galaxy derived from imaging observations (e.g., Bertin & Toniazzo 1995). They are also significantly below the value, 0.43 ± 0.06 $M_{\odot}$ yr^{-1}, inferred from O VI observations in the UV band by Bregman et al. (2001). Similar discrepancies between mass deposition rates inferred from imaging data and those allowed by the RGS spectra have been found for massive cooling flow in clusters of galaxies (Peterson et al. 2001; Kaastra et al. 2001; Tamura et al. 2001) and had even been suggested by the original ASCA data (cf. Makishima et al. 2001).

4. Discussion

Giant elliptical galaxies are the most massive and the oldest stellar systems in the universe. Analyses of their stellar spectra, and their evolution with time has indicated that most of the stars formed at very high redshift. There is little evidence of any significant star formation within the last 5 Gyrs. The hot X-ray emitting ISM in these systems is the repository of the total mass loss from stellar winds, planetary nebulae, and supernovae. As such, its metal abundances are very sensitive to both the abundances in the stars themselves, and to the Type Ia supernova rate.

Previous analyses of X-ray emission from ellipticals (cf., Arimoto et al. 1997) presented some fundamental challenges to our understanding of the formation and evolution of these systems. Given that the stars are believed to be supermetal rich, and that supernovae only add metals to the interstellar gas, it was expected that the X-ray spectra would yield metal abundances well in excess of solar. The general picture was that the low-Z elements should be strongly skewed to those of massive supernovae (Type IIs), while Fe should show a particular enhancement, as high as 2 - 5 times solar, due to the contributions of Type Ia supernovae.

The first quantitative test of these predictions came with ASCA, which provided moderate resolution X-ray spectra, suitable for identifying broad emission "humps" associated with each of the major elemental constituents. Contrary to expectations, fits to ASCA spectra invariably yielded significantly subsolar abundances (Matsumoto et al. 1997). In the intervening years, a variety of suggestions have been offered to explain this discrepancy: Problems with the iron L-shell atomic physics in the available spectral codes (Arimoto et al. 1997; Matsushita, Ohashi & Makishima 2000); multi-temperature distributions in the emitting gas (Buote 1999); abundance gradients and metallicity dependent supernova rates (Finoguenov & Jones 2000); excess helium abundance (Drake

1998). The multitude of possibilities arises from the fact that the available ASCA data did not have sufficient spatial or spectral resolution to constrain the situation in any real detail. Abundance information could only be derived by global fits to the entire spectrum, which are known to produce misleading results if the assumptions invoked are invalid. In fact, as shown in Matsushita et al. (1997), the iron abundance can be increased to ~ 1 solar if systematic errors are allowed at 20% level in the spectral fittings to ASCA data.

It is worth noting that the abundance patterns of the stars in giant ellipticals are also subject to uncertainties. In particular, Trager et al. (2000) and Kobayashi and Arimoto (1999) have shown that one can really only reliably determine the relative abundances of the alpha elements, and the Fe/alpha ratio. It appears that there is often a steep alpha element abundance gradient in the inner regions of the galaxy, without an accompanying gradient in the iron abundance. Such effects call into question the simple chemical enrichment models that have previously been developed for these systems.

The XMM-Newton RGS observations of NGC 4636 presented here provide the most accurate and unambiguous abundance determinations to date for the ISM of a giant elliptical galaxy. We have shown that there is a weak, but measurable, temperature gradient in the inner regions of the ISM. In addition, we have shown that resonance scattering of the high oscillator strength iron lines is non-negligible, consistent with expectations given the measured central electron density in the gas. Both of these effects are very important, and must be properly taken into account in the derivation of abundance constraints from the X-ray spectrum. The high statistical quality of our data, coupled with the high spectral and spatial resolution that the RGS provides, makes our abundance and temperature constraints far more robust than any previous determinations.

Nevertheless, our derived values: O/Ne ~ 0.7 solar, O/Mg ~ 0.8 solar, O/Fe ~ 0.6 solar, and Fe ~ 0.87 solar, are still difficult to reconcile with the chemical enrichment

models. In particular, these values do not match the Type Ia and Type II models in Gibson, Lowenstein and Mushotzky (1997), nor any linear superposition of these models. The iron abundance has been increased significantly compared with those previous measurements, but it is still lower than the theoretical predictions. One possible explanation is that iron has been escaping from the ISM, as inferred by the observed large scale metal abundance gradient in NGC 4636 (Mushotzky et al. 1994; Matsushita et al. 1997). We believe that our results and future investigations set a standard to which new models of the evolution of giant ellipticals should be compared.

Equally puzzling is the clear lack of a measurable cooling flow in the ISM of NGC 4636. It has been well accepted for over fifteen years (e.g., Nulsen et al. 1984) that the central regions of giant elliptical galaxies should exhibit strong cooling flows. For NGC 4636, our inferred central density indicates a cooling time of less than 10^8 years. This is compatible with the sound crossing time evaluated at the local sound speed, which means that the gas should be cooling as fast as it possibly can. There are no obvious sources of heating in this gas - Type Ia supernovae and stellar winds provide too little energy. In addition, recent Chandra observations (Lowenstein et al. 2001) have shown that there is no active nucleus present in this galaxy. A previous outburst from a now dormant active nucleus could provide the required heat (Jones et al. 2001), but it is unclear yet how common such outbursts might be.

However, as we have shown the weakness of the Fe XVII and O VII lines, and the absence of gas at temperatures less than 500 eV are in strong disagreement to the cooling flow models. There is only a weak temperature gradient and no other evidence of multiphase gas. In particular, the higher resolution RGS data do not support the conclusions of Buote & Fabian (1998), which were derived from ASCA observations of this source.

As noted in §3.3, problems with cooling flow models have also emerged from

XMM-Newton RGS observations of clusters of galaxies. The issue is actually more severe for NGC 4636 given the wealth of discrete spectral lines available in the lower temperature range appropriate to elliptical halos. It is conceivable that our data could be compatible with a model in which some unknown form of rapid cooling occurs, radiating most of the energy in the ultraviolet. The fact that the O VI measurements from FUSE (Bregman et al. 2001) suggest a higher mass deposition rate than allowed by our O VII upper limits might argue for such a picture. Turbulent mixing layers (Begelman & Fabian 1990) could possibly accomplish this by entraining the X-ray gas and rapidly mixing it down to temperatures of order 10^5 K. Additionally, the distortion of the emission measure distribution by adiabatic compression (Nulsen 1998) might conceivably explain our results given the relatively narrow temperature range we are sampling. Regardless of the eventual explanation, this observation does demonstrate that the discrepancies with cooling flow predictions occur even on small scales, not only for the massive flows in galaxy clusters.

This work was supported by a grant from NASA to Columbia University for XMM-Newton mission support and data analysis. We wish to thank other key members of the RGS team for their advice on instrument calibration and data analysis issues. H. Xu is also partially supported by the National Science Foundation of China (Grant No. 19803003) and the Ministry of Science and Technology of China (Project 973).

REFERENCES

Anders, E., & Grevesse, N. 1989, Geochim. Cosmochim. Acta, 53, 197

Arimoto, N., Matsushita, K., Ishimaru, Y., Ohashi, T., & Renzini, A. 1997, ApJ, 477, 128

Awaki, H., et al. 1994, PASJ, 46, L65

Behar, E., Cottam, J., & Kahn, S. M. ApJ, 548, 966

Begelman, M. C., & Fabian, A. C. 1990, MNRAS, 244, 26

Bertin, G., & Toniazzo, T. 1995, ApJ, 451, 111

Bregman, J. N., Miller, E. D., & Irwin, J. A. 2001, ApJ, 553, L125

Brown, G. V., Beiersdorfer, P., Liedahl, D. A., Widmann, K., & Kahn, S. M. 1998, ApJ, 502, 1015

Brown, G. V., Beiersdorfer, P., Chen, H., Chen, M. H., & Reed, K. J. 2001, ApJ, 557, L75

Buote, D. A. 1999, MNRAS, 309, 685

Buote, D. A., & Fabian, A. C. 1998, MNRAS, 296, 977

Cavaliere, A., & Fusco-Femiano, R. 1976, A&A, 49, 137

den Herder, J. W., et al. 2001, A&A, 365, L7

Drake, J. J. 1998, ApJ, 496, L33

Ferrarese, L., et al. 2000, ApJ Supplement, 128, 431

Finoguenov, A. & Jones, C. 2000, ApJ, 539, 603

Gibson, B. K., Loewenstein, M., & Mushotzky, R. F. 1997, MNRAS, 290, 623

Johnstone, R. M., Fabian, A. C., Edge, A. C., & Thomas, P. A 1992, MNRAS, 255, 431

Jones, C., Forman, W., Vikhlinin, A., Markevitch, M., David, L., Warmflash, A., Murray, S., & Nulsen P. E. J. 2001, ApJ Letters, submitted

Kaastra, J. S., Ferrigno, C., Tamura, T., Paerels, F. B. S., Peterson, J. R., & Mittaz, J. P. D. 2001, A&A, 365, L99

Kobayashi, C., & Arimoto, N. 1999, ApJ, 527, 573

Laming, J. M., et al. 2000, ApJ, 545, L161

Loewenstein, M., Mushotzky, R. F., Angelini, L., Arnaud, K. A., & Quataert, E. 2001, ApJ, 555, L21

Makishima, K., et al. 2001, PASJ, 53, 401

Matsumoto, H., Koyama, K., Awaki, H., Tsuru, T., Loewenstein, M., & Matsushita, K. 1997, ApJ, 482, 133

Matsushita, K., Ohashi, T., & Makishima, K. 2000, PASJ, 52, 685

Matsushita, K. 2001, ApJ, 547, 693

Matsushita, K., Makishima, K., Rokutanda, E., Yamasaki, N. Y., & Ohashi, T. 1997, ApJ, 488, L125

Murphy, E. M., Lockman, F. J., Laor, A., & Elvis, M. 1996, ApJS, 105, 369

Mushotzky, R. F., Loewenstein, M., Awaki, H., Makishima, K., Matsushita, K., & Matsumoto, H. 1994, ApJ, 436, L79

Mushotzky, R. F., et al. 2001, in preparation

Nulsen, P. E. J., Stewart, G. C., & Fabian, A. C. 1984, MNRAS, 208, 185

Nulsen, P. E. J. 1998, MNRAS, 297, 1109

Peterson, J. R., et al. 2001, A&A, 365, L104

Peterson, J. R., Jernigan, J. G., & Kahn, S. M. 2001, in preparation

Smith, R. K., Brickhouse, N. S., Liedahl, D. A., & Raymond, J. C. 2001, ApJ, 556, L91

Smith, R. J., Lucey, J. R., Hudson, M. J., Schlegel, D. J., & Davies, R. L. 2000, MNRAS, 313, 469

Tamura, T., et al. 2001, A&A, 365, L87

Trager, S. C., Faber, S. M., Worthey, G., & Gonzalez, J. J. 2000, AJ, 119, 1645

This manuscript was prepared with the AAS LaTeX macros v5.0.

Table 1: Measured line fluxes from the central 2' of NGC 4636

$\lambda_{\rm observed}$	λ_0^*	Ion	Upper Level		Lower Level		Flux
(Å)	(Å)		Configuration	J_U	Configuration	J_L	(10^{-4} ph s^{-1} cm^{-2})
12.1	12.132	Ne^{9+}	$2p_{3/2}$	3/2	1s	1/2	2.24
	12.137	Ne^{9+}	$2p_{1/2}$	1/2	1s	1/2	
14.2	14.208	Fe^{17+}	$2p_{1/2}2p^3_{3/2}3d_{3/2}$	5/2	$2p^2_{1/2}2p^3_{3/2}$	3/2	1.90
	14.208	Fe^{17+}	$2p_{1/2}2p^3_{3/2}3d_{5/2}$	3/2	$2p^2_{1/2}2p^3_{3/2}$	3/2	
14.3	14.256	Fe^{17+}	$2p_{1/2}2p^3_{3/2}3d_{3/2}$	1/2	$2p^2_{1/2}2p^3_{3/2}$	3/2	1.45
	14.267	Fe^{19+}	$2s2p^2_{1/2}2p_{3/2}3s$	3/2	$2s2p^2_{1/2}2p^2_{3/2}$	5/2	
14.4	14.373	Fe^{17+}	$2p_{1/2}2p^3_{3/2}3d_{3/2}$	5/2	$2p^2_{1/2}2p^3_{3/2}$	3/2	1.85
14.5	14.534	Fe^{17+}	$2p^2_{1/2}2p^2_{3/2}3d_{5/2}$	5/2	$2p^2_{1/2}2p^3_{3/2}$	3/2	2.25
	14.571	Fe^{17+}	$2p^2_{1/2}2p^2_{3/2}3d_{5/2}$	3/2	$2p^2_{1/2}2p^3_{3/2}$	3/2	
15.0	15.014	Fe^{16+}	$2p_{1/2}2p^4_{3/2}3d_{3/2}$	1	$2p^2_{1/2}2p^4_{3/2}$	0	3.56
15.3	15.261	Fe^{16+}	$2p^2_{1/2}2p^3_{3/2}3d_{5/2}$	1	$2p^2_{1/2}2p^4_{3/2}$	0	1.66
16.1	16.004	Fe^{17+}	$2p^2_{1/2}2p^2_{3/2}3s$	3/2	$2p^2_{1/2}2p^3_{3/2}$	3/2	1.99
	16.071	Fe^{17+}	$2p^2_{1/2}2p^2_{3/2}3s$	5/2	$2p^2_{1/2}2p^3_{3/2}$	3/2	
	16.110	Fe^{18+}	$2s^22p_{1/2}2p^2_{3/2}3p_{1/2}$	2	$2s2p^2_{1/2}2p^3_{3/2}$	2	
16.8	16.780	Fe^{16+}	$2p_{1/2}2p^4_{3/2}3s$	1	$2p^2_{1/2}2p^4_{3/2}$	0	2.33
17.0	17.051	Fe^{16+}	$2p^2_{1/2}2p^3_{3/2}3s$	1	$2p^2_{1/2}2p^4_{3/2}$	0	2.77
17.1	17.096	Fe^{16+}	$2p^2_{1/2}2p^3_{3/2}3s$	2	$2p^2_{1/2}2p^4_{3/2}$	0	2.89
19.0	18.967	O^{7+}	$2p_{3/2}$	3/2	1s	1/2	1.96
	18.973	O^{7+}	$2p_{1/2}$	1/2	1s	1/2	

$*$ λ_0 is the wavelength measured with EBIT for iron (Brown et al. 1998, 2000), or calculated in HULLAC for other elements (cf. Behar et al. 2001).

Table 2: Fe XVII line ratios measured in NGC 4636 and Capella

	$2p_{3/2}-3s/2p_{1/2}-3s$ I(17.1)/I(16.8)	$2p_{1/2}-3d_{3/2}/2p_{3/2}-3d_{5/2}$ I(15.0)/I(15.3)	$2p_{3/2}-3s/2p_{1/2}-3d_{3/2}$ I(17.1)/I(15.0)
NGC 4636	2.30 ± 0.18	2.31 ± 0.18	1.40 ± 0.13
Capella*	2.37 ± 0.19	2.42 ± 0.22	1.65 ± 0.11
APEC (600 eV)**	2.28	3.49	1.01

$*$ From Behar et al. 2001.

$**$ Predictions of APEC model (Smith et al. 2001).

Table 3: Best-fit spectral model (errors are 90% confidence)

$kT_{\rm min}$ (keV)	$kT_{\rm max}$ (keV)	α	R_c (arcmin)	n_0 ($\rm cm^{-3}$)	χ^2_r
0.53 ± 0.03	0.71 ± 0.02	5.8 ± 0.3	42 ± 4	0.125 ± 0.005	1.18
Metal abundances in solar units					
Fe	O	Mg	Ne	N	
0.87 ± 0.05	0.50 ± 0.05	0.65 ± 0.07	0.70 ± 0.07	1.00 ± 0.10	

Figure Captions

Fig.1–The raw, extracted RGS spectrum of NGC 4636 (black), plotted as a function of wavelength. The data from both first and second spectral orders from RGS1 and RGS2 have been added together in constructing this histogram. The best fit model, allowing for a temperature gradient and accounting for resonance line scattering effects, is plotted in red. The residuals to the model fit are plotted below.

Fig.2–The ratios of various emission lines (as indicated in the panels), plotted as a function

of position in the cross-dispersion direction. The data (with appropriate error bars) are plotted as crosses. The predictions of the best-fit spatial/spectral model are plotted as diamonds.

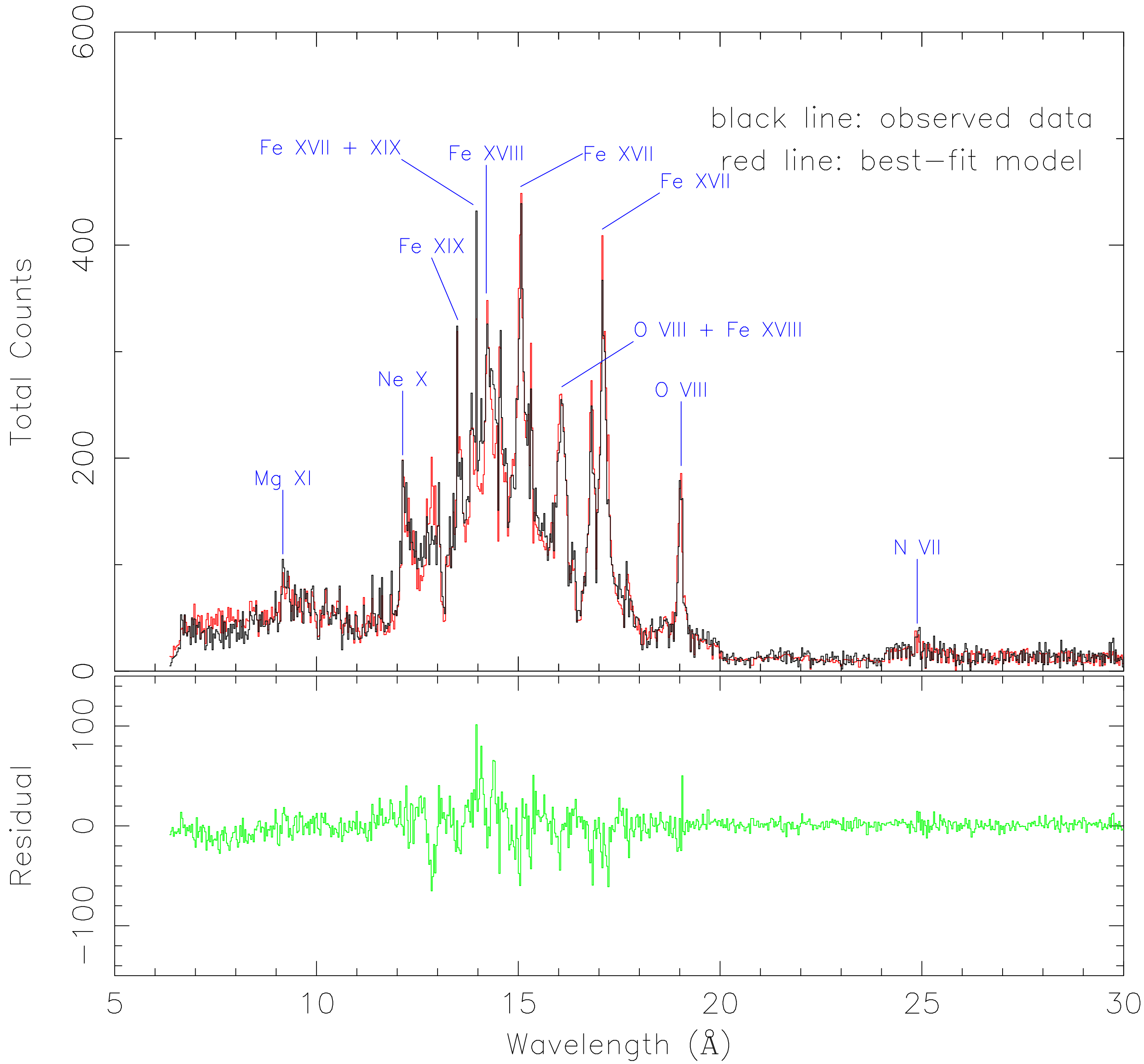

black line: observed data
red line: best−fit model
Fe XVII + XIX
Fe XVIII
Fe XVII
Fe XVII
Fe XIX
O VIII + Fe XVIII
Ne X
O VIII
Mg XI
N VII
Total Counts
Residual
Wavelength (Å)

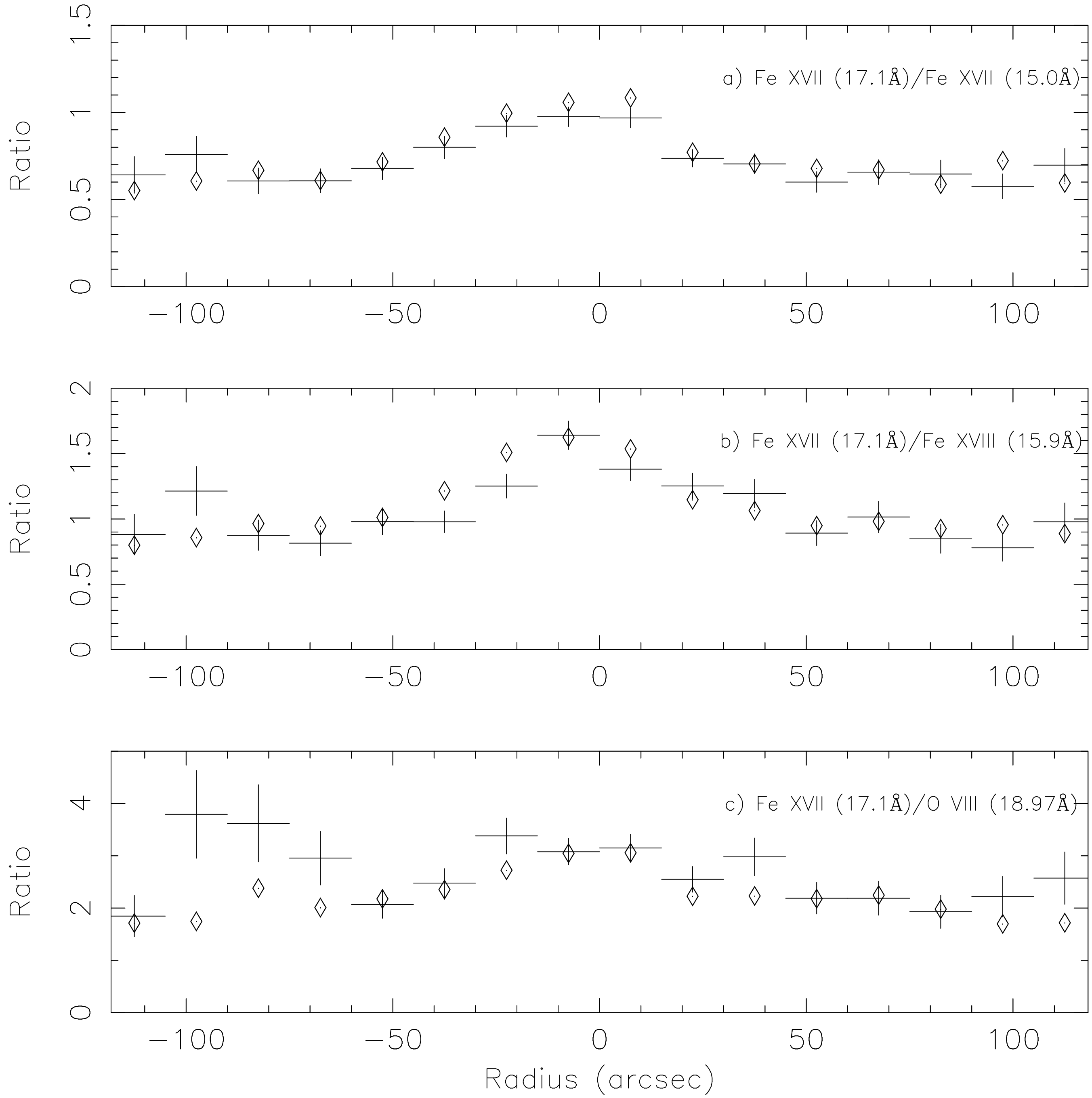
a) Fe XVII (17.1Å)/Fe XVII (15.0Å)
b) Fe XVII (17.1Å)/Fe XVIII (15.9Å)
c) Fe XVII (17.1Å)/O VIII (18.97Å)
Ratio
Radius (arcsec)